JOURNAL OF AIRCRAFT
Vol. 48, No. 4, July–August 2011

Multi-Aircraft Dynamic Continuous Descent Approach Methodology for Low-Noise and Emission Guidance

S. Alam,* M. H. Nguyen,* H. A. Abbass,† and Chris Lokan‡
University of New South Wales, Australian Defence Force Academy, Canberra, New South Wales 2600, Australia
and
M. Ellejmi§ and S. Kirby¶
EUROCONTROL Cooperative Network Design, 91222 Brétigny-sur-Orge, France

DOI: 10.2514/1.C031241

Continuous descent approaches can significantly reduce fuel burn and noise impact by keeping arriving aircraft at their cruise altitude for longer and then having a continuous descent at near-idle thrust with no level-flight segments. The continuous descent approach procedures are fixed routes that are vertically optimized. With the changing traffic conditions and variable noise-abatement rules, the benefits of continuous descent approach are not yet fully realized. In this paper, a methodology is proposed to generate aircraft-specific dynamic continuous descent approach routes that are both laterally and vertically optimized for noise, emission, and fuel. The methodology involves discretizing the terminal airspace into concentric cylinders with artificial waypoints and uses enumeration and elimination (based on aircraft performance envelope) from one waypoint to another to identify all the possible routes. From the resulting set of possible continuous descent approach routes, routes are identified that represent the best tradeoff on the given objectives. The dynamic continuous descent approach algorithm is implemented in an air traffic simulator for the Sydney, Australia, terminal area. Dynamic continuous descent approach, as compared with a typical continuous descent approach, shows a 14.96% reduction in noise, 11.6% reduction in NO_x emission, and 1.5% reduction in fuel burn. The throughput capacity of transition airspace is also investigated for multiple flights performing continuous descent approach operation for different traffic distributions. The methodology incorporates a delay algorithm that uses the flight's estimated time of arrival at the intermediate approach fix, which allocates a conflict-free continuous descent approach route by searching through possible routes.

Nomenclature

b	=	boundary-layer thickness, cm
C_f	=	first thrust-specific fuel-consumption coefficient, kg/ min /kN
C_{f3}	=	first descent fuel-flow coefficient, kg/ min
C_{f4}	=	second descent fuel-flow coefficient, ft
$C_{T_c,1}$	=	first aircraft-specific maximum-climb thrust coefficients, N
$C_{T_c,2}$	=	second aircraft-specific maximum-climb thrust coefficients, ft
$C_{T_c,3}$	=	third aircraft-specific maximum-climb thrust coefficients, $1/\text{ft}^2$
$CT_{\text{des,ld}}$	=	landing thrust coefficient, dimensionless
dt	=	time step
EIHC	=	emission index of hydrocarbon, g/kg
EICO	=	emission index of carbon monoxide, g/kg
EINO_x	=	emission index of nitrogen monoxide, g/kg
flap(t)	=	aircraft flap setting at time t, deg
g	=	acceleration due to gravity, kt/s
h	=	aircraft altitude, ft
$h(t)$	=	aircraft altitude at time t, ft
m	=	simulated aircraft mass, kg
m_{ref}	=	reference mass, kg
$T_{\text{max climb,ISA}}$	=	maximum-climb thrust at standard atmosphere conditions, N
$V(t)$	=	aircraft velocity at time t, m/s
V_{min}	=	minimum landing speed, m/s
V_{stall}	=	stall speed at the reference mass, m/s
$W(t)$	=	aircraft weight at time t, kg
γ	=	flight-path angle, rad

Presented as Paper 2010-202 at the 29th AIAA Digital Avionics Systems Conference (DASC), Salt Lake City, UT, 3–7 October 2010; received 17 September 2010; revision received 16 March 2011; accepted for publication 18 March 2011.

*Research Fellow, Defence & Security Applications Research Center.
†Professor and Director, Defence & Security Applications Research Center.
‡Senior Lecturer, School of Engineering & Information Technology.
§Project Manager, Early Demonstration & Evaluation Platform.
¶Analyst, Cooperative Network Design/Performance and Methods.

I. Introduction

WITH the continued growth in air traffic, airport runways are expected to handle a higher volume of traffic [1,2]. A consequence is that aircraft noise and local air quality become a concern for residents living in areas surrounding airports [3]. Noise restrictions are often placed on airports (for example, London's Heathrow and Sydney's Kingsford Smith), which can limit daily operations [4].

Noise-efficient operations, such as continuous descent approaches (CDAs), can significantly reduce the noise impact of landing aircraft by keeping aircraft at higher altitudes on approach to the airport and by reducing power during descent [5,6]. Research into the economic and environmental costs and benefits of using continuous descent approaches (as opposed to step descent) showed significant reduction in noise footprints and aviation emission [7,8]. CDA is also considered as one of the building blocks for Single European Sky ATM Research and Next Generation Air Transportation System [9].

A typical CDA procedure starts from an initial approach fix (IAF) at approximately 10,000 to 8000 ft and around 30 to 25 nm to touchdown. When cleared for the CDA, the aircraft starts its descent in such a way that the instrument landing system (ILS) intercept point is reached at 2500–2000 ft [final approach fix (FAF)] with idle or near-idle power setting. This airspace is usually referred to as transition airspace. In CDA, the aircraft descends to touchdown with

a glide slope of 3 deg along an optimized lateral flight path. In the conventional CDA approach, this lateral path is fixed.

In addition to the need for a mandatory certification for pilots and aircraft to conduct a CDA operation, the CDA routes are fixed and published well in advance. They are essentially arrival routes that are vertically optimized. With the changing traffic conditions and noise-abatement rules (to distribute noise evenly in surrounding areas or to shift it to uninhabited areas), the full benefits of CDA operations is not fully realized [10].

In this paper we propose a methodology to generate dynamic CDA routes. Dynamic CDA are aircraft-specific, starting from initial approach fix to final approach fix. The word *dynamic* refers to the fact that two aircraft in the same approach airspace can follow two different trajectories: there is no standard arrival (STAR); in practice, each aircraft will receive its dynamic CDA by data link before starting its descent. These CDA trajectories are generated by discretizing the terminal airspace into concentric cylinders with artificial waypoints and uses enumeration and elimination (based on aircraft performance envelope) from one waypoint to another to identify all the possible routes. For each transition a variety of metrics are computed, including noise, emission, and fuel burn. From the resulting set of possible CDA routes, those routes are identified that represent the best tradeoff on the given objectives.

The proposed methodology is integrated into a high-fidelity air traffic simulator (ATOMS) [11]. The methodology uses real-time aircraft position and defined objectives to generate trajectories that can be converted into a set of artificial waypoints for continuous descent in transition airspace for a given set of objectives such as noise, emission, and fuel consumption.

The dynamic CDA approach is developed with consideration for future integration with flight management systems. To accommodate for real-time updates to the lateral path, the algorithm outputs a set of CDA trajectories with trajectory change points that represent the possible optimal tradeoffs between competing objectives. These CDA trajectories can then be displayed to the approach/tower air traffic control (ATC), where a controller can select a solution based on operational preferences and uplink the chosen trajectory to the aircraft.

The proposed methodology is then extended to the multiple-aircraft scenario, by blocking the artificial waypoints generated for the first aircraft and making them inaccessible for other aircraft for a period of time based on estimated time of arrival (ETA) of the first aircraft at its respective artificial waypoints.

II. Background

Environmental impacts due to aviation operations in the vicinity of airports have become a serious concern to the community [12]. Aircraft noise and emission have generated numerous complaints and public litigations from residents near airports. This is affecting the progress of commercial aviation, any efforts of airport expansion, and new runway developments. The result is a lack of enough runways at major airports, which in turn increases fuel consumption and airspace congestion. This leads to increased aircraft emission, which affects both the natural environment and human health [13].

Researchers have been evaluating ways to alleviate noise and emission problems associated with increases in air traffic. Continuous descent approaches are noise- and fuel-efficient terminal approaches that have been a research topic over the last few years and are being explored by several governments, industry, and academic institutions.

A continuous descent approach is defined as "an aircraft operating technique in which an arriving aircraft descends from an optimal position with minimum thrusts and avoids level flight to the extent permitted by the safe operation of the aircraft and compliance with published procedures and ATC instructions" [14]. Thus, in CDA, the descent is with no level-altitude segments, which are common in traditional step descent approaches. The goal of developing a CDA is to keep the aircraft thrust as low as possible and the aircraft at higher altitudes for as long as possible [15]. An ideal CDA allows the engines to be at idle thrust during most of the descent. Figure 1 shows

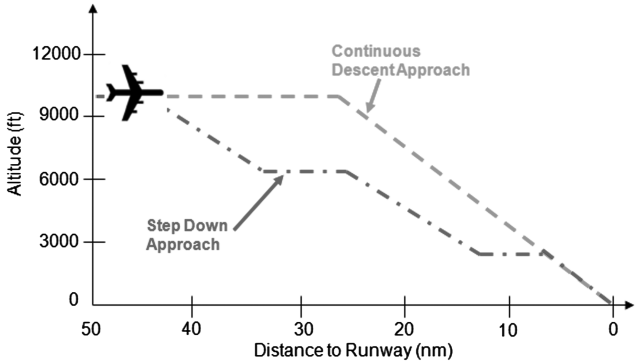

Fig. 1 Conceptual representation of step descent approach and continuous descent approach.

the conceptual representation of a conventional step descent approach and a continuous descent approach, which typically starts at 10,000 ft and around 25–30 nm from the touchdown point [7].

After the aircraft begins to descend past top-of-descent, lower thrust, fuel consumption, and noise results from eliminating level-altitude segments. In CDA operations, the thrust is near idle during most of the descent; therefore, significant deceleration is achieved by using flaps.

CDA flight tests at Louisville International Airport in the United States with B767 and B757 aircraft have shown a 50% reduction in acoustic energy, compared with traditional approach routes [8]. Significant fuel savings were also shown, which would greatly benefit both the environment and the airlines over time. CDA operations have been implemented at some airports during low-density traffic operations, such as Heathrow in London, Schiphol in Amsterdam, and Brisbane in Australia.

III. Dynamic Continuous Descent Approach

In ideal conditions, the CDA route should be an optimized 3-D trajectory that is generated and shared between controllers and the pilot in real time by taking into account noise, emission, traffic, and wind conditions. With increased onboard computing power, advances in digital data transmission, and proposed real-time data link between controllers and pilots (CDPLC), uplinking and downlinking of trajectories is possible [16]. This makes the realization of real-time CDA route generation a near possibility.

In the near future, controllers will be able to define their objectives and their relative priority and uplink them to the approaching aircraft. An onboard system can then use them to generate a set of CDA trajectories that can then be downlinked for ATC's approval.

Finding dynamic CDA trajectories in transition airspace can thus be seen as a path-planning problem in three dimensions. In air traffic management this problem attains unique dimensions, due to aircraft performance constraints posed on it in approach phase, such as limited maneuverability (low thrust), speed restrictions, and altitude constraints. Apart from the hard safety constraints, the other competing objectives are to minimize noise, emission, and fuel consumption.

A. Problem Search Space

As shown in Fig. 2, we define the problem search space (transition airspace) as a set of five concentric cylinders (to equally divide transition airspace with 5 nm safety separation) with runway (touchdown point) at the center. The height of the transition airspace for research purpose is set to 10,000 ft and the radius is set to 25 nm. The outermost cylinder (denoted as ring 4) is of radius 25 nm [transition airspace radius (TAR)] with subsequent inner cylinders (rings 3, 2, 1, and 0) spaced at equal distance as calculated in Eq. (1). The outermost cylinder height is 10,000 ft corresponding to the start altitude of CDA and subsequent inner cylinders are vertically separated by 2000 ft. Thus, the transition airspace is divided into five

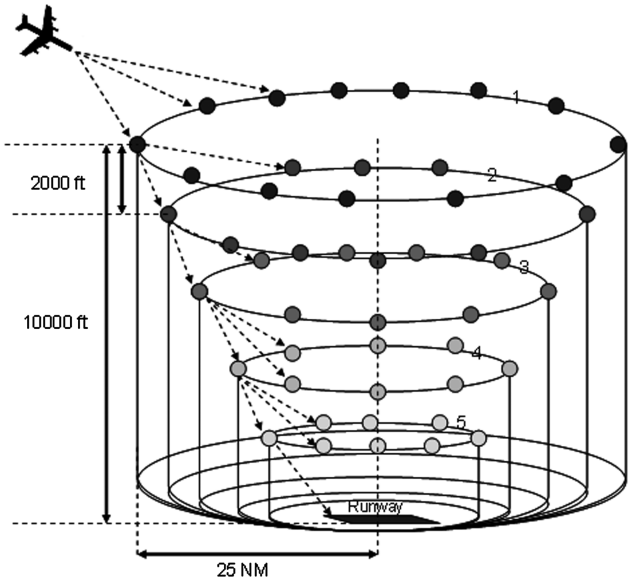

Fig. 2 Conceptual representation of division of transition airspace into concentric circles and wedges acting as trajectory change points for dynamic CDA trajectory generation.

levels, with each level divided into 2000 ft to give a typical jet aircraft enough vertical height to maneuver given low-thrust setting:

$$\text{ring radius} = \frac{\text{TAR} \times (\text{ring number} + 1)}{5} \tag{1}$$

Each cylinder has wedges that represent transition points from one level to another. These wedge points are spaced 1.5 nm apart along the circumference of rings from each other for safe separation between approaching aircraft [17]. The number of wedges for each cylinder and the angle between them are computed based on Eqs. (2) and (3).

The number of wedges for a given cylinder is calculated as follows:

$$\text{number of wedges} = \frac{2\pi \times \text{ring radius}}{\text{separation distance}} \tag{2}$$

The angle between the wedges is calculated as follows:

$$\text{wedge angle} = \frac{2\pi}{\text{number of wedges}} \tag{3}$$

Using a transition airspace radius of 25 nm and a separation distance of 1.5 nm, Eqs. (1) and (2) give the number of wedge points as 104, 83, 62, 41, and 20 for rings 4, 3, 2, 1, and 0, respectively.

At 2000 ft before touchdown it is assumed that the aircraft follows the final approach path on the ILS glide scope and lands. The transition from one wedge point to other wedge point is based on individual aircraft performance parameters derived from EUROCONTROL's Base of Aircraft Data (BADA) [18]. All the wedge points on the outermost cylinder (representing the boundary of the transition airspace) are accessible for an approaching flight. Similarly, all the wedge points on the innermost cylinder represent final approach fixes that lead to a ILS touchdown point.

The algorithm performs a full enumeration of the search space from CDA entry point (initial approach fix) in the outermost ring to exit points (final approach fix) in the cylindrical transition airspace. This enumeration leads to a large number of possible paths from IAF to FAF. Finding feasible solutions in such a large search space can be computationally expensive, from safety and time perspectives. To reduce the number of searches we need to reduce the states in the search space without compromising solution quality. Only those transitions from a wedge on one ring to a wedge on the next ring that are within the aircraft's performance envelope (turn angle, vertical speed) are considered; the rest are eliminated. This reduces the search space, and it also leads to a safety-inherent design for dynamic CDA route planning.

By preprocessing to eliminate infeasible transitions in the search space, the search is guaranteed to produce feasible solutions. We eliminate the state space recursively, starting from the entry point and doing forward enumeration on different layers. At each layer we eliminate states that violate the aircraft performance parameters, and then we move to the following layer. With each transition, from one wedge to the next, the objective values (emission, noise, and fuel burn) are computed until the FAF points are reached.

B. Problem Definition

The problem can then be stated as follows: given a 3-D cylindrical grid (transition airspace) of dimensions i (ring), j (level), k (wedge), an entry point A (initial approach fix) and a set of exit points B (final approach fixes) find the set of routes (trajectories) between A and B that minimizes the given objectives (noise, emission, and fuel).

This search space is then discretized in a cylindrical grid of $i \times j \times k$ wedge points, which forms the transition airspace around the airport. Each cell in the grid forms a state in the search graph. The arcs of the graph represent possible transitions from one state to another. The state space is then processed by removing those states that violate aircraft performance parameters for continuous descent approaches, such as aircraft turn angle, maximum rate of descent, and speed constraints given the available thrust, using BADA.

The resulting 3-D cylindrical grid is stored in a 3-D array data structure as an enumerated state space where each element of the array represents a point in the grid. The pseudocode for this is presented in Algorithm 1.

Every array element stores the information about its position (latitude, longitude, and altitude) and all the immediate next links (that do not violate the aircraft performance envelope) from that point in the grid. Further, for each link the array element stores the heading change required, altitude change required, distance between the two, time, noise generated, emission generated, and fuel flow.

IV. Optimization Function Formulation

We have considered three minimization objectives: noise is the noise generated by the aircraft airframe for a given CDA trajectory, emission is the emission generated by the aircraft for a given CDA trajectory, and fuel burn is the fuel consumed by an aircraft for a given CDA trajectory.

Aircraft noise includes airframe noise and engine noise, but only airframe noise is calculated in this study, because in most modern aircraft, airframe noise is a significant contributor to aircraft noise during the continuous descent approach. Sources of airframe noise include flaps, slats, wing, tails, and landing gear [19]. Since the engines are already on low-thrust settings a CDA operation and are thus a constant contributor to the overall aircraft noise, the main source of variation is the airframe noise.

Algorithm 1 Pseudocode for state-space processing

```
   Require: aircraft performance database d: (rate of heading change, rate
      of climb and descent, altitude ceiling, max. bank angle, max. turn
      angle, max. vertical speed)
   Grid G with i × j × k dimensions
   Exit node position in the grid (sink)
1: for node in G do
2:    Compute the turn angle, altitude change, rate of heading change
         required, rate of altitude change required, vertical speed required
         from each node (xyz) to the grid point (ijk) in G
3:    if transition from node xyz to grid point ijk violates D, then
4:       Eliminate the link
5:    else
6:       Retain the link
7:    end if
8: end for
9: return grid G with links within aircraft safety envelope
```

A. Noise Optimization Formulation

The objective function of the noise optimization problem is a weighted integral of noise perceived at the ground level during the approach phase in the transition airspace. In particular, the weight factor considers the population and noise sensitivity of communities near an airport. Constraints on the optimization include initial and terminal conditions, the maximum feasible flap, velocity and altitude change rate, and a set of specified waypoints (wedge points) during the CDA. Therefore, the noise optimization problem, to minimize noise given aircraft characteristics, could be formulated as follows:

$$\min f = \int_0^t W(t)\text{noise}(V(t), h(t), \text{flap}(t), t)\,\mathrm{d}t \tag{4}$$

where $W(t)$ is the aircraft weight at time t, $V(t)$ is the aircraft velocity at time t, $h(t)$ is the aircraft altitude at time t, and flap(t) is the flap setting at time t.

Noise models that are commonly used in airframe noise acoustics studies include Lilley's model [20]; Federal Aviation Administration (FAA) integrated noise model [21]; DLR, German Aerospace Center model [22]; and overall sound pressure level (OASPL) model [19]. We have used the OASPL model in the paper, as it is most appropriate for the dynamic CDA procedure, which uses the concept of transition airspace modeled as cylinders. The OASPL model aggregates the noise in the whole cylinder, whereas Lilley's model computes noise from a single reference point (an observer in the ground). In terms of noise impact on the community surrounding the airport area, OASPL is more suitable.

In the OASPL model, airframe noise is a function of altitude $h(t)$, velocity $v(t)$, flap setting flap (t)), boundary-layer thickness b, and wingspan $\delta(t)$ [23]. It can be expressed as

$$\begin{aligned}\text{OASPL} &= 50\log v(t) - 20\log h(t) + C_f \times \text{flap}(t) \\ &\quad + 10\log\delta(t) \times b + \text{const}\end{aligned} \tag{5}$$

where C_f is the coefficient of thrust in approach configuration for a given aircraft. The effect of landing gear (increases in the drag) is captured by approach thrust coefficient C_f. The term const is 10 log (measurement period). The measurement period (seconds) is equal to simulation run time.

During continuous descent approach, the altitude and velocity of the aircraft decrease gradually. Therefore, no abrupt noise changes occur. Thus, we can define the noise cost function of the optimization problem in Eq. (4) as

$$\begin{aligned}\text{noise}_{ij} &= W \times \sum_t [50\log v(t) - 20\log h(t) + C_f \times \text{flap}(t) \\ &\quad + 10\log\delta(t) \times b + \text{const}]\end{aligned} \tag{6}$$

where W is the weight factor. The subscript i, j in the noise function denotes the cumulative noise between two wedge points on successive rings.

B. Aircraft Fuel-Burn Computation

Total approach fuel burn is estimated by integrating fuel burn at each second. A thrust-specific fuel-flow model of BADA with correction for aircraft mass was used. When the aircraft engine is set to idle thrust during approach and landing, the fuel burn per second is given by [18]

$$\text{fuel rate} = \frac{C_{f3}}{60} \times \left(1 - \frac{3.2080 \times h}{C_{f4}}\right) \tag{7}$$

where C_{f3} is first descent fuel-flow coefficient and C_{f4} is second descent fuel-flow coefficient for an aircraft, derived from the BADA aircraft operation performance file.

The fuel flow for each transition is computed as

$$\text{fuel flow}_{ij} = \text{time in leg}_{ij} \times \text{fuel rate} \tag{8}$$

C. Aircraft Emission Computation

Four major aircraft emissions, CO_2, HC, NO_x and CO are computed. The emission computation process is divided into two phases, below 3000 ft and above 3000 ft. Below 3000 ft, the emission calculation is based on the ICAO Engine Exhaust Emissions Data Bank [24]. Above 3000 ft, the emission calculation is also based on the ICAO Engine Exhaust Emissions Data Bank, but emission factors are adapted to the atmospheric conditions at altitude by Boeing emission method 2 (BEM2) [25], which calculates emission indices based on fuel flow and ICAO (International Civil Aviation Organization) certification data. ICAO data at the four certified power settings at sea-level conditions are used to compute resulting emissions while correcting for atmospheric conditions. BEM2 computes flight emissions using the measured fuel flow and the engine ICAO data sheets as a base. It allows for ambient pressure, temperature, humidity, and Mach number.

These emissions are formulated as

$$\text{CO}_2 = \text{no. of engines} \times \text{EICO}_2 \times \text{fuel flow} \tag{9}$$

$$\text{CO} = \text{no. of engines} \times \text{EICO} \times \text{fuel flow} \tag{10}$$

$$\text{HC} = \text{no. of engines} \times \text{EIHC} \times \text{fuel flow} \tag{11}$$

$$\text{NO}_x = \text{no. of engines} \times \text{EINO}_x \times \text{fuel flow} \tag{12}$$

where EINOx, EICO, and EIHC are emission indices of NO_x, CO, and HC, respectively, derived from the ICAO Engine Exhaust Emission Data Bank, and

$$\text{EICO}_2 = \text{EICO}_{2,\text{ideal}} - \frac{44}{28}\text{EICO}$$

where $\text{EICO}_{2,\text{ideal}}$ is 3156 g, the 44/28 ratio represents their different molar masses, and fuel flow is in grams/second.

Respective emissions for each transition in the cylindrical grid (from node i to node j) are computed as

$$\text{emission}_{ij} = \text{time in leg}_{ij} \times \text{emission} \tag{13}$$

We have used nitrogen monoxide (NO_x) emission as the objective value for emissions. However, other pollutants (HC, CO, and CO_2) computed in the study could also be used. We chose NO_x because of its impact on local air quality and its major influencing substances on global warming [26]. NO_x is a precursor of ground-level ozone (O_3); hence, an elevated O_3 level may result through a chemical reaction with oxygen in the presence of sunlight [26]. Respiratory complaints are the main effects related to elevated concentrations of NO_x around the airport area [27].

The overall optimization function F can then be stated as

$$\min F = \sum_i \sum_j \text{noise}_{i,j}, \text{emission}_{i,j}, \text{fuel}_{i,j} \tag{14}$$

The aerodynamics and flight configuration parameters are controlled by the air traffic simulator ATOMS. The simulator uses the BADA aircraft performance model to control and coordinate the thrust, flap configuration, and speed parameters. The fuel and noise models discussed above takes aerodynamic and flight parameter inputs from the air traffic simulator and compute the appropriate values. These values are then used in the overall optimization function [Eq. (14)]. The noise model accounts for vertical speed, aircraft altitude, flap angle, and wing span [Eqs. (4) and (5)]. Similarly, the fuel and emission models [28] also account for aerodynamic parameters.

V. Aircraft Performance Model

The following changes were made in the aircraft performance model of ATOMS to implement CDA approaches and to improve the fidelity of the simulation.

A. Final Approach Speed

The minimum landing speed $V_{\min}$ is now calculated as follows:

$$V_{\min} = 1.3 \times V_{\text{stall}} \sqrt{\frac{m}{m_{\text{ref}}}} + 10.0 \text{ kt} \tag{15}$$

where 1.3 is a factor recommended by the BADA manual [18] for all aircraft operations, V_{stall} is the stall speed at the reference mass m_{ref}, and m is the simulated aircraft mass.

B. Deceleration Rate

The BADA manual [18] recommends a maximum longitudinal acceleration/deceleration of 2.0 ft/s^2 (118 kt/s), and this value was previously implemented in ATOMS as the maximum deceleration, regardless of flight-path angle. To compensate for a descending aircraft, $g\gamma$ was subtracted from the maximum longitudinal acceleration, where g is the acceleration due to gravity in knots per second (kt/s) and γ is the flight-path angle in radians; for a 3 deg flight-path angle, the $g\gamma$ term is approximately equal to 1.0 kt/s. This change was necessary to properly simulate the diminished deceleration capabilities that are characteristic of CDA operations.

The deceleration rates are also affected by the flap configuration. BADA aircraft-specific flap configuration for approach and landing and corresponding stall speeds were used. The landing gear was fixed at 3000 ft and was reflected in increased coefficient of drag during landing.

C. Descent Thrust

Once the aircraft has descended below 10,000 ft, it changes configuration as soon as the airspeed falls below threshold $V_{\min}$. At the same time, the thrust setting is also changed as follows: if $h < 10,000$ ft and $V < V_{\min} + 10.0$ kt,

$$T_{\text{des,ld}} = C_{T\text{des,ld}} \times \left(\frac{m}{m_{\text{ref}}}\right) \times T_{\text{max climb,ISA}} \tag{16}$$

where $C_{T\text{des,ld}}$ is the landing thrust coefficient (dimensionless), m_{ref} is the reference mass of aircraft (tons) h (feet) is the aircraft altitude, $T_{\text{max climb,ISA}}$ is the maximum-climb thrust at standard atmosphere conditions, which is computed as follows:

$$T_{\text{max climb,ISA}} = C_{T_c 1} \times \left(1 \frac{h}{C_{Tc,2}} + C_{Tc,3} \times h^2\right) \tag{17}$$

where $C_{T_c 1}$, $C_{Tc,2}$, and $C_{Tc,3}$ are aircraft-specific maximum-climb thrust coefficients in newtons, feet, and $1/\text{ft}^2$, respectively.

VI. Numerical Experiments and Results

The transition airspace and CDA procedure was modeled in ATOMS, and numerical experiments were conducted to evaluate the methodology.

For the single flight, a B737-400 aircraft on a flight from Melbourne to Sydney, arriving at Sydney terminal area with 34L as the arrival runway, was simulated in descent phase. The aircraft is equipped with two CFM56-3C-1 engines with a nominal weight (58,000 kg). Two flap settings (15 and 30 deg) are used. International Standard Atmosphere (ISA) conditions are assumed for performance, fuel, noise, and emission calculations. ISA defines air temperature, pressure, temperature, and other atmospheric parameters as functions of altitude. Neither local deviations from ISA conditions nor winds are considered for our experiment purposes.

A single aircraft was investigated first. The algorithm was used to identify a set of possible dynamic CDA trajectories. The dynamic CDA routes were then compared on noise, emission, and fuel burn with the same flight conducting a typical fixed CDA procedure (MANFA ONE arrival) at the Sydney airport. The results of this experiment are presented in this section of the paper.

A second experiment investigated a scenario with multiple flights performing CDA operation, to gain insight into the throughput capacity of transition airspace. Those results are presented in Sec. VII.

A. Dynamic CDA Trajectories

Once the aircraft is in descent mode after top-of-descent, 25 nm before the transition airspace, the algorithm searches for possible wedge points on the transition airspace boundary. The algorithm computes the entry wedge point (initial approach fix) that has least distance between the aircraft and the wedge points of the outermost cylinder and that involves minimum aircraft heading change. It then determines the exit wedge points (final approach fixes) that can be achieved from the IAF. For research purposes, the runway is assumed to be the center point of the concentric rings; thus, all the points on the innermost circle become the target set for exit.

We first demonstrate the generation of transition airspace and the fully enumerated state space. Figure 3 shows all the possible wedge links in the cylindrical transition airspace before removing infeasible states. Figure 4 illustrates the wedge links after removing infeasible transition states that violate aircraft performance constraints. This shows a significant reduction in the state space.

Based on the IAF point, all the possible paths are generated. For each trajectory change point in a path, the emission, noise, and fuel values are computed as described above, and these are aggregated for each CDA trajectory. There are 11,254 possible routes generated from the 104 wedge points on the outermost ring to the 20 wedge points on the innermost ring.

Each of these routes represents a unique path or CDA trajectory, starting from a wedge (IAF) on the outermost ring and ending on a final approach fix point in the innermost ring, The entry wedge point (IAF) of an aircraft in the cylinder is based on which IAF point is closest to its current flight path and requires the least deviation from its current heading.

The example aircraft has ring 4, level 4, and wedge 14 as the closest IAF. The methodology generates 101 possible solutions (dynamic CDA trajectories) for the aircraft from the selected IAF (starting from 4-4-14) to all the possible exit points (FAF) in the given transition airspace. Figure 5 shows the 3-D view of all the CDA trajectories starting from the transition airspace entry point (IAF) to the final approach point (FAF), which is 2000 ft above touchdown.

Out of 101 possible dynamic CDA trajectories, four trajectories are nondominated solutions. The concept of nondominated [29] is generally used to compare two solutions a and b: If $f(a)$ is no worse for all objectives than $f(b)$ and wholly better for at least one objective, it is said that a dominates b. A set F of solutions is said to be a nondominating set if no element of the set dominates any other. These solutions are also called Pareto-optimal, as no other feasible solution dominates them. The set of all Pareto-optimal solutions is known as the Pareto set P; solutions in the Pareto set represent the possible tradeoffs between competing objectives.

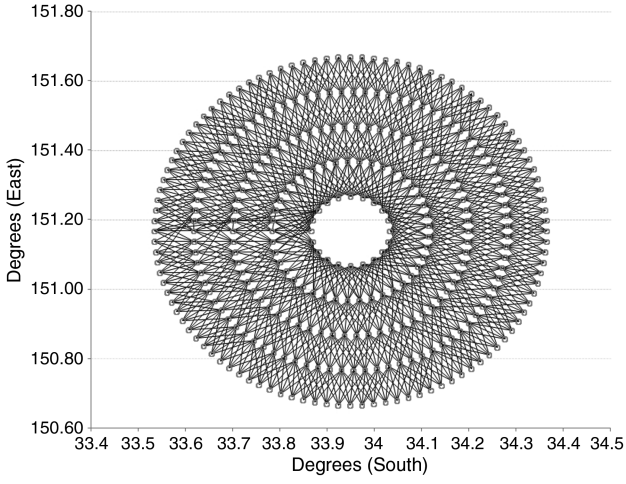

Fig. 3 Wedge links in the cylindrical transition airspace before removing the infeasible states.

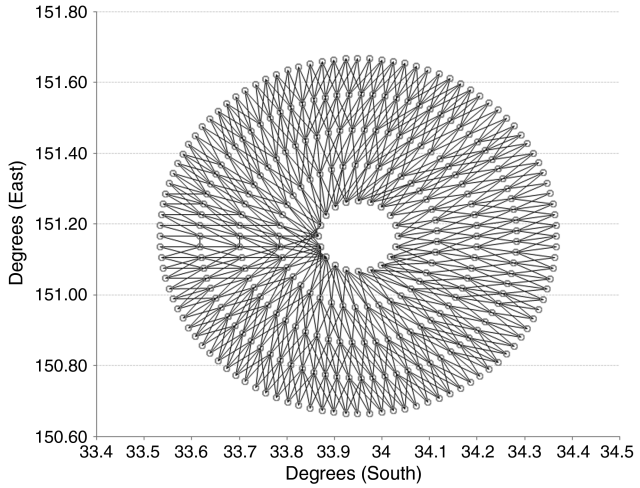

Fig. 4 Wedge links in the cylindrical transition airspace after removing infeasible states.

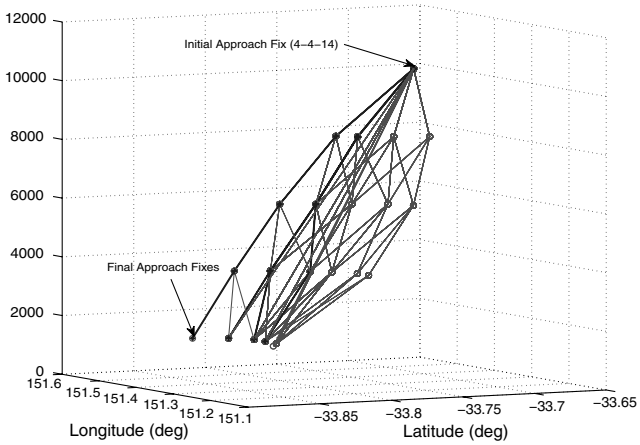

Fig. 5 Three-dimensional view of dynamic CDA trajectories generated from one of the entry point (4-4-14) in the transition airspace by the algorithm. The figure also highlights the four nondominated trajectories.

Mathematically, it can be stated as [30] follows: a vector $\mathbf{u} = (u_1, \ldots, u_m)$ is said to dominate $\mathbf{v}$ if and only if $\forall\ i\epsilon\{1, \ldots, m\}$, $u_i \leq v_i \wedge \exists j\epsilon\{1, \ldots, m\}$: $u_j < v_j$. Thus, a solution $x\epsilon N$ is said to be nondominated or Pareto-optimal with respect to the whole set N if and only if there is no other solution $x'\epsilon N$ for which $F(x')$ dominates $F(x)$. Figure 5 illustrates the nondominated solution trajectories among the set of all feasible trajectories.

The Pareto solution set and their route indexes are presented in Table 1. Ring in Table 1 implies the cylinder number, where 4 is the outermost and 0 is the innermost cylinder. Level implies the altitude level, where 4 is 10,000 ft and 0 is 2000 ft. The aircraft chooses any one of the nondominated solutions and after reaching the final approach point the aircraft descends directly to the designated runway.

Table 1 also shows the objective values for each of the four trajectories. It shows the emission, fuel flow and noise for each representative CDA trajectory. Each CDA route generated by the algorithm has some trade off between noise, emission, and fuel consumption. Figure 6 shows the 3-D plot for the three objective values for all the feasible solutions, as well as the Pareto-optimal solutions.

The CDA trajectories generated are within the aircraft performance bounds. Figure 7 shows the altitude, flap configurations, thrust, speed profile, fuel flow and acceleration from 80 nm till touchdown for one of the Pareto-optimal dynamic CDA trajectories. Fifteen-degree flaps are extended at approximately 10 nm to threshold, 30 deg flaps are extended at approximately 7 nm to threshold, and thrust is almost idle until 23 nm to touchdown. The aircraft under goes deceleration many times, as compared with the step-down approach, to maintain the required speed profile. The generated trajectory maintains the 3 deg flight-path angle with speed and altitude constraints while executing the selected CDA approach.

B. Comparison of Dynamic CDA Trajectories with Fixed CDA Trajectory

We compared the performance [measured on noise, emission (NO_x) and fuel] of Dynamic CDA trajectories with the fixed CDA trajectory flown using a STAR route for the Sydney (Kingsford Smith Airport) MANFA ONE arrival.

As shown in Fig. 8, we modeled the BOREE-BEROW-OVILS-MAJAR-MANFA-JAKLN-LISHA-SUZAN STAR route in the ATOMS simulator. The aircraft follows the STAR route using continuous descent approach and lands east of runway 16R/34L. The same experiment and flight settings were used as for dynamic CDA trajectories.

To generate the dynamic CDA trajectories, ring 4, level 4, and wedge 68 (4-4-68) is chosen as the transition airspace entry point (IAF) for the inbound aircraft, as it coincides with the fixed CDA entry point for MANFA ONE arrival STAR fix at an altitude of 10,000 ft. From this IAF point until the final approach fix (2000 ft) the noise, emission, and fuel burn are computed and compared for the two approaches. Figure 9 shows the fixed CDA trajectory for Sydney MANFA ONE arrival as compared with the nondominated solution trajectories generated by the algorithm.

Dynamic CDA approach generated 67 possible routes from IAF point (4-4-68) to final approach fixes. Out of them five were nondominated solution trajectories on noise, emission (NO_x) and fuel-burn objectives. Table 2 shows the five nondominated solution trajectories and their objective values.

Table 3 compares one of the nondominated dynamic CDA routes with the fixed CDA route on the noise, emission, and fuel-burn objectives and illustrates the savings achieved by the former approach.

For the Dynamic CDA we see a reduction of 14.96% in airframe noise, 11.99% reduction in NO_x emission and 1.5% reduction in fuel burn. Though the savings in fuel burn was not that large, since the aircraft was already in low-thrust setting and there was not much room for reduction, from an environmental prospective, the reduction was still important.

VII. Multiple-Aircraft Scenario

CDA operations are usually conducted at night and/or in low traffic conditions. One reason is that for CDA, the landing interval has to increase to guarantee sufficient spacing between aircraft on the final landing segment [31]. The increased landing interval is

Table 1 Objective values of four Pareto-optimal solution trajectories out of 101 CDA trajectories generated by the algorithm.

Route (ring-level-wedge)	Noise, db	Emission NO_x, kg	Fuel, kg
4-4-14 → 3-3-11 → 2-2-8 → 1-1-4 → 0-0-0	63.56	198.68	355.77
4-4-14 → 3-3-11 → 2-2-8 → 1-1-5 → 0-0-1	64.01	198.62	355.72
4-4-14 → 3-3-11 → 2-2-8 → 1-1-5 → 0-0-2	64.97	198.60	355.67
4-4-14 → 3-3-12 → 2-2-9 → 1-1-6 → 0-0-3	65.97	198.60	355.67

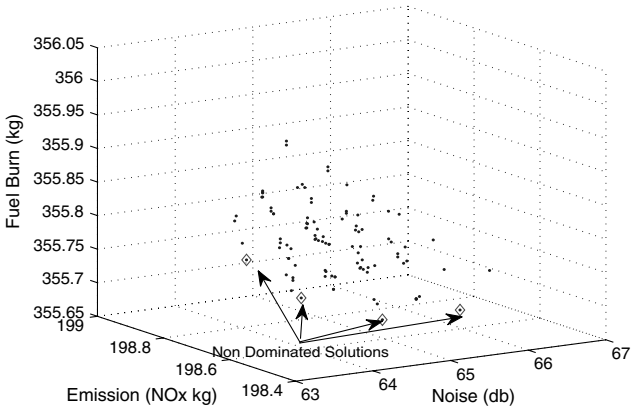

Fig. 6 Three-dimensional plot of the three objective values (fuel, emission, and noise) for all the feasible dynamic CDA trajectories. The four Pareto-optimal solutions are highlighted by diamonds.

necessary because of the large dispersion in aircraft approach speeds. Moreover, since the aircraft conducting CDA operation is in ideal or near-ideal thrust, the increased spacing allows for thrust increase to deal with sudden changes in wind, missed approaches, or any other reason that requires vectoring the aircraft.

For the proposed dynamic CDA methodology, we looked into different air traffic scenarios with 100 flights, each having different activation timings and traffic distributions. We then evaluated the performance of the proposed methodology in terms of throughput capacity, delay between outer marker and initial approach fix, delay between initial approach fix and final approach fix, and cumulative values for emission, noise, and fuel.

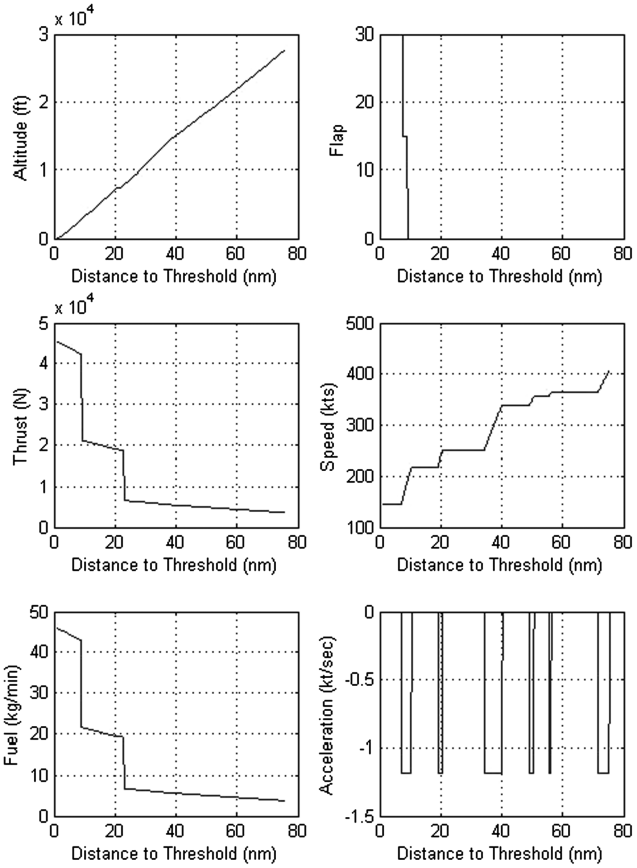

Fig. 7 Distance to threshold plots for aerodynamic parameters and fuel flow for continuous descent approach trajectory (80 nm to touchdown) for one of the CDA trajectories.

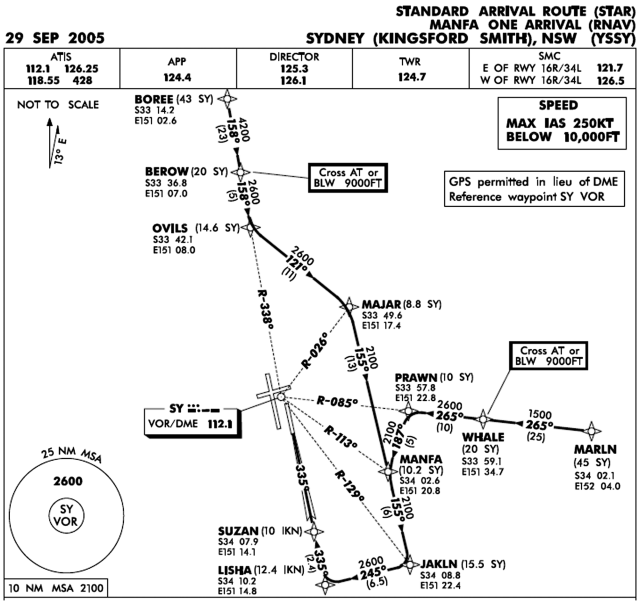

Fig. 8 STAR chart of MANFA ONE arrival [33] at Sydney International Airport, which is modeled in ATOMS for CDA procedure simulation.

A. Sequencing Multiple Flights

We incorporated a delay algorithm, which uses the ETA of the flight at its designated IAF and then at each artificial waypoint in the transition airspace until the FAF, to sequence the flights. A time window is assigned based on aircraft type (light, medium, and heavy) at each artificial waypoint, so that any subsequent flights does not occupy the same waypoints in that given time frame. This is achieved by time-blocking these waypoints, which are then eliminated during the link enumeration process. This ensures that no two flights occupy the same waypoint in a given time window.

The dimensions of the cylindrical grid (transition airspace) are fixed, but the links (and their objective values) from one level to the other and from one wedge to the other are always specific to an aircraft. Aircraft are allocated on the CDA route on a first-come, first-served (FCFS) basis. If the route is not available, the aircraft is slowed down by 20 kt if the speed is within its flight envelope (stall speed). Otherwise, the aircraft is put on hold. Figure 10 illustrates the time-delay algorithm component in the dynamic CDA generation process.

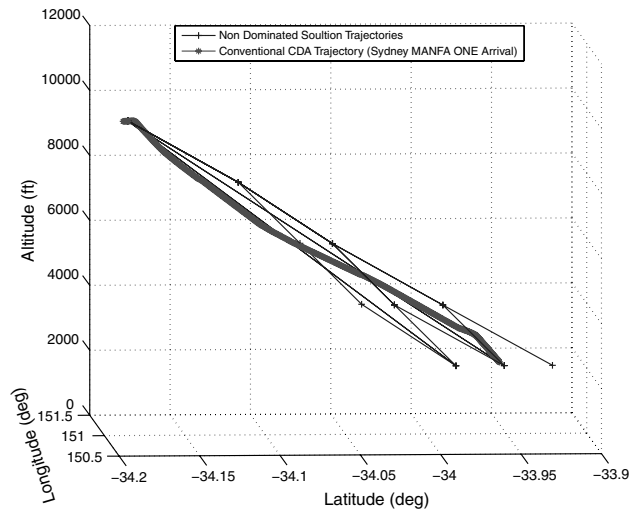

Fig. 9 Conventional CDA trajectory for Sydney MANFA ONE arrival as compared with the nondominated solution trajectories generated by the algorithm.

Table 2 Objective values of five nondominated solution trajectories out of 67 CDA dynamic trajectories generated by the algorithm for entry point 4-4-68 corresponding to MANFA STAR fix

Route (ring-level-wedge)	Noise, db	Emission NO_x, kg	Fuel, kg
4-4-68 → 3-3-55 → 2-2-41 → 1-1-27 → 0-0-14	64.99	198.60	355.69
4-4-68 → 3-3-55 → 2-2-42 → 1-1-28 → 0-0-14	63.98	198.61	355.69
4-4-68 → 3-3-55 → 2-2-42 → 1-1-28 → 0-0-15	63.52	198.64	355.73
4-4-68 → 3-3-55 → 2-2-42 → 1-1-29 → 0-0-15	63.02	198.66	355.73
4-4-68 → 3-3-55 → 2-2-42 → 1-1-29 → 0-0-16	62.57	198.69	355.78

There are four main components of the time-delay algorithm:

1) A flight is selected for CDA route allocation when it reaches the outer marker (50 nm from IAF) using FCFS. This is based on the flight's ETA at the destination airport.

2) An IAF is selected based on minimum distance and minimum flight-path deviation. The selected IAF is checked for availability (whether open or closed) in the time window, given the aircraft's ETA at that IAF. If the IAF is not available, another possible IAF is selected.

3) If no IAF is open, given the flight's ETA at any of the IAF, the algorithm generates a command to reduce speed. It then checks whether the reduced speed is within aircraft stall limits given the altitude and flight phase (approach/descent). If the proposed speed is with stall limits, then ETA at the destination is recalculated and the flight is repositioned in the FCFS list. Otherwise, the aircraft is set in hold status, i.e., frozen in simulation. However, the flight parameters (including noise, emission, and fuel) are continuously computed during the hold process.

4) Based on the selected CDA route for the flight, the algorithm updates the cylindrical grid for all the wedge points (artificial waypoints) that form part of the dynamic CDA route. We have used time-based separation [32], where the algorithm sets the wedge point as closed and assigns a busy status (for the ETA of the flight and the wake-separation criterion), as shown in Table 4. Once the aircraft crosses the waypoint, the status is set to open.

This class of aircraft is based on its maximum takeoff weight (MTOW) characteristics: light aircraft have MTOW of 7000 kg or less; medium aircraft have MTOW of greater than 7000 kg, but less than 136,000 kg; and heavy aircraft have MTOW of 136,000 kg or greater.

For the experiments we have used time-based separation [32], as shown in Table 4. We have used only heavy aircraft (90 s separation) to demonstrate the concept, but it can be easily extended to any category of aircraft as long it is equipped with suitable avionics that support CDA operations.

B. Traffic Distributions

Figure 11 illustrates the overall airspace where the activation point is set to 150 nm from the outer marker. The outer marker is 50 nm away from the initial approach fix. The flights get activated at their designated activation point based on the traffic distribution. Once the flight reaches the outer marker, the optimization process starts.

As illustrated in Fig. 12, three traffic distributions have been developed to get variation in arrival traffic distribution. The three traffic distributions are based on typical one day's arrival traffic distributions into Sydney International Airport, at different times of the day. The traffic distributions are generated using a probability distribution function. The circular grid is divided into eight equal regions, 45 deg each, which we call octants.

Table 3 Comparisons of noise, emission, and fuel values of one of the nondominated trajectories of dynamic CDA with traditional CDA using fixed STAR route

Route	Noise, db	Emission NO_x, kg	Fuel, kg
Dynamic CDA	64.99	198.60	355.69
Fixed-route CDA	76.43	225.68	361.21
Reduction (%)	14.96	11.99	1.5

1) In traffic distribution 1, all the incoming traffic is uniformly distributed in all the eight octants.

2) In traffic distribution 2, the incoming traffic is uniformly distributed in octants II, IV, VI, and VIII.

3) In traffic distribution 3, all the incoming traffic is uniformly distributed in octants II and III.

Figure 13 illustrates the flight activation points for the three traffic distributions in experimental airspace.

C. Activation Time

Flights are activated in the airspace using an interarrival time that is determined by a Poisson process. So any two successive flights have a time interval between them that is derived by a Poisson distribution. We have used four intervals, based on the heavy–heavy aircraft separation of 90 s. The activation time is determined by a Poisson process with values of m set to 0, 30, 60, and 90. For example, if interarrival time is 0, this means that all the flights are activated at the same time; an interarrival time of 30 implies that the activation time between two successive flight is Poisson-distributed with a mean of 30 s; and so on.

The combination of three traffic distributions and four activation time gives us 12 air traffic scenarios, where each scenario is composed of 100 flights.

As illustrated in Fig. 14, a uniform random number generator first selects the octant (from 1 to 8) based on the traffic distribution. For example, if the traffic distribution is 3, then it will only select points from octants II and III; otherwise, the random number is regenerated. There are 104 activation points equally divided in the eight octants, so there are 13 points in each octant. Once the octant from which flights will be activated is identified, the activation points are selected using a uniform random number. Thus, if octant I is selected by the above process, a uniform random number generator will then select an activation point (0–12) for a flight in this octant.

As an example, Fig. 15 shows the ATOMS simulation snapshot for one of the scenarios (evenly distributed traffic in space, and interarrival time of 0).

D. Results and Analysis

We collected three metrics for dynamic CDA operations in a high-density traffic environment for each of the 16 scenarios described above (recall that each scenario involves the same number and same type of aircraft):

1) The throughput of transition airspace (flights per minute) gives the number of flights that can be processed by the system per minute. It is estimated by dividing the number of flights processed by the system by the time difference between first flight activation time and last flight landing time:

$$\text{throughput} = \frac{\text{flights}}{\text{activation time}_{\text{FF}} - \text{landing time}_{\text{LF}}} \tag{18}$$

where FF implies the first flight activated in the scenario and LF implies the last flight that landed in the scenario.

2) The average flight delay time from outer marker to IAF is a measure of hold-induced delay. It is estimated by taking the difference between the ETA of the flight to the IAF and actual time of arrival (ATA) to the IAF from the outer marker, averaged over 100 flights:

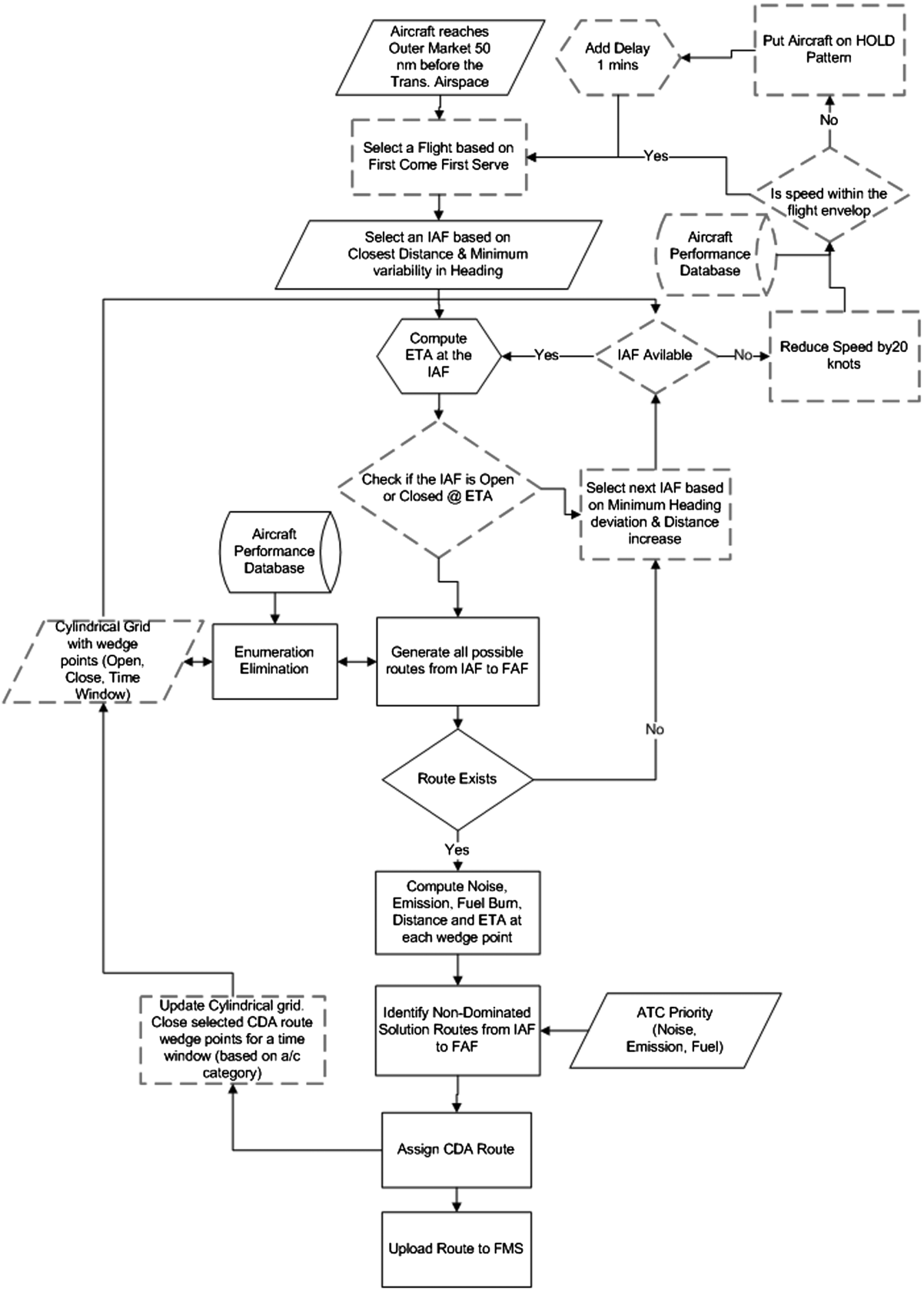

Fig. 10 Flowchart showing the delay algorithm components (dotted line) in the dynamic CDA generation process.

$$\text{delay} = \left[\frac{1}{N}\Sigma_{i=1}^{100}(\text{ATA}_i - \text{ETA}_i)\right]_{\text{IAF}}^{\text{OM}} \tag{19}$$

3) The cumulative noise, emission (NO_x), and fuel burn for all 100 aircraft are collected from the outer marker until final approach fix.

1. Throughput

Figure 16 shows the throughput of the system for the three traffic distributions with different interarrival timings. It can be seen that when the interarrival time is 0, then Traffic distribution 2 (traffic distributed in alternate octant) gives the best throughput. As expected

Table 4 Time-based separation for CDA arrivals at each occupied wedge point between leading and following aircraft in the cylindrical grid

	AC/follow AC		
Lead	Heavy, s	Medium, s	Light, s
Heavy	90	110	145
Medium	70	70	125
Light	70	70	70

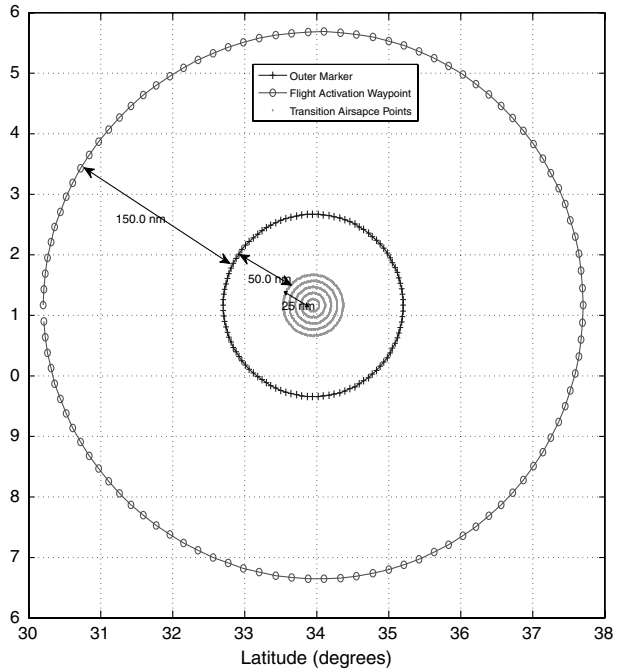

Fig. 11 Optimization airspace showing activation points that are 150 nm from the outer and marker outer-marker points that are 50 nm from the initial approach fix.

traffic scenario 3 where all the flights are from octants 3 and 4 has the least throughput.

However, interestingly, when the interarrival time between flights is increased to 30 s scenario 3 gives the best throughput. With 90 s of interarrival timing the traffic distribution do not make much difference in the throughput of the system.

2. *System Delay*

Figure 17 shows the average flight delay from outer marker to initial approach fix for different interarrival timings for the three traffic distributions.

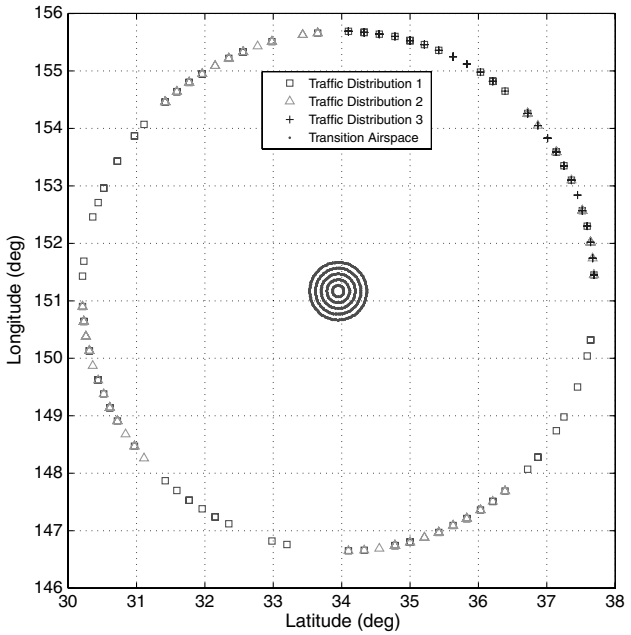

Fig. 13 Flight activation positions for the three traffic distributions in the eight octants.

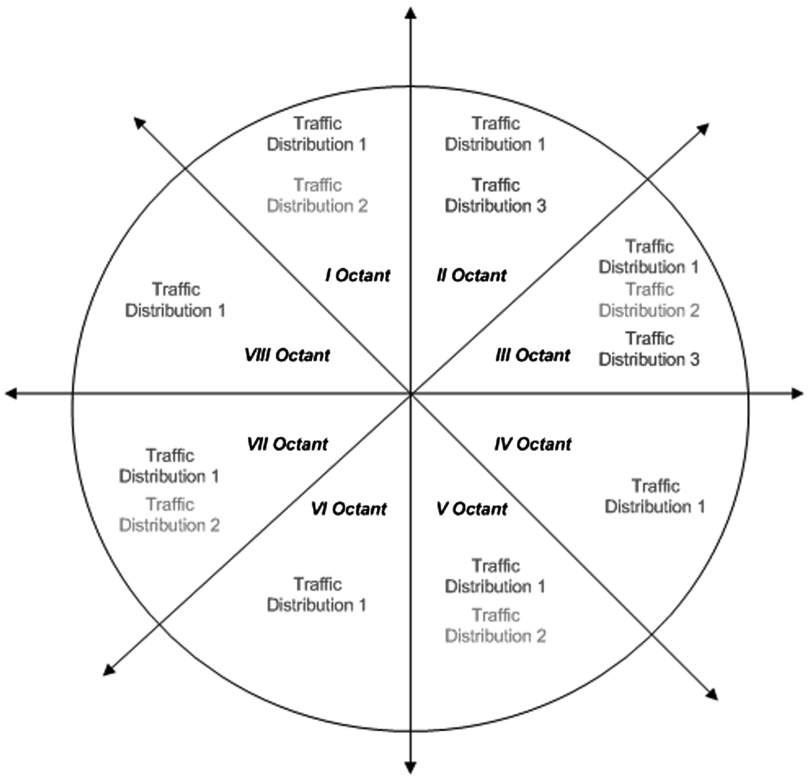

Fig. 12 Traffic distributions of incoming traffic in eight octants.

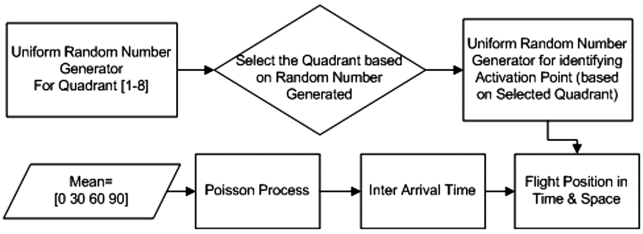

Fig. 14 Process showing the generation of flight position in space and time-based on traffic scenario.

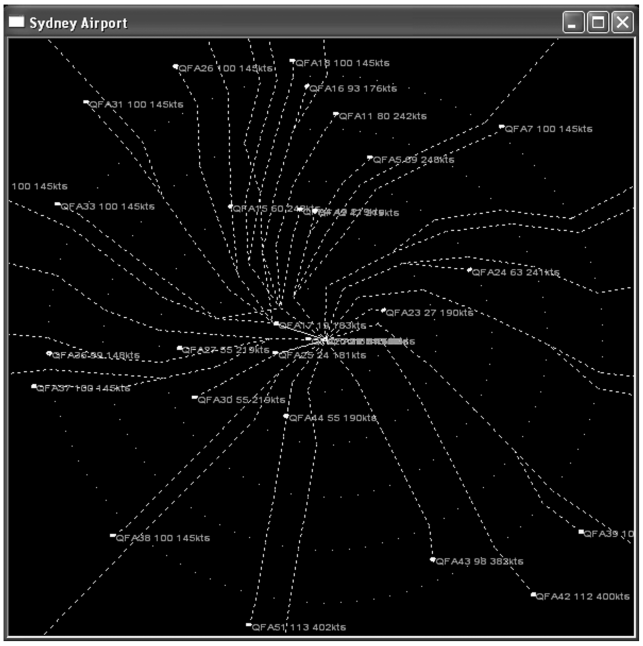

Fig. 15 Snapshot of traffic scenario simulation in ATOMS for evenly distributed traffic in space and interarrival time of 0.

It can be seen that for traffic distribution 3, (a typical morning scenario when all the oceanic flights from the United States are lined up for entry into the Sydney terminal airspace), the average flight delay is highest with the interarrival timings of 0 and 30 s. By increasing the interarrival time to 60 s scenario 3 gives the least delay and the delay in scenario 1 is significantly increased. For evenly distributed traffic (traffic distribution 1), the best performance is achieved with 30 s of interarrival time.

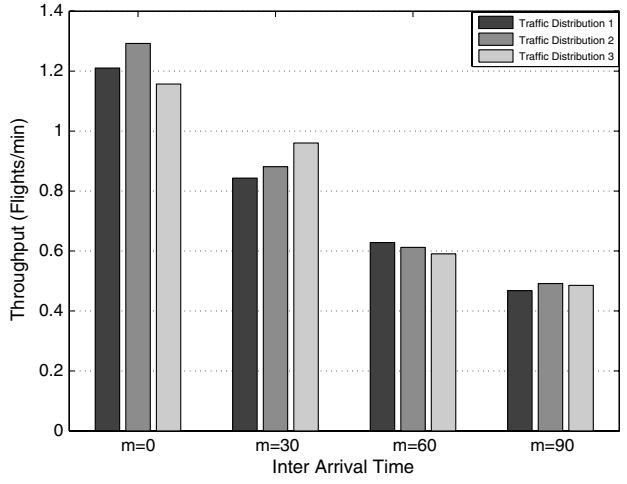

Fig. 16 Throughput of the transition airspace for the three traffic distributions with different interarrival timings.

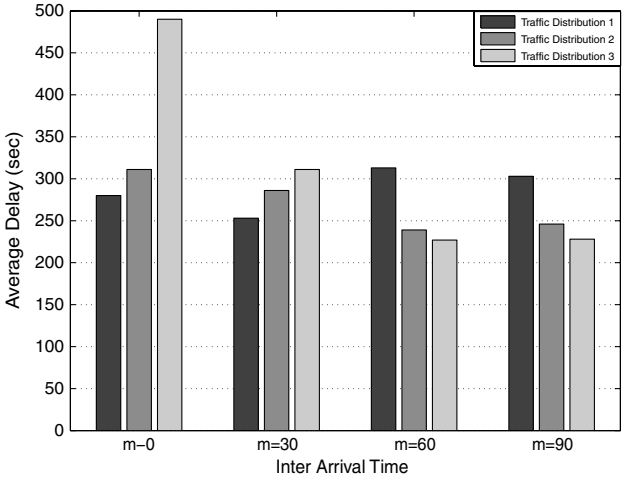

Fig. 17 Delays (seconds) from the outer marker to IAF for the three traffic distributions with different interarrival timings.

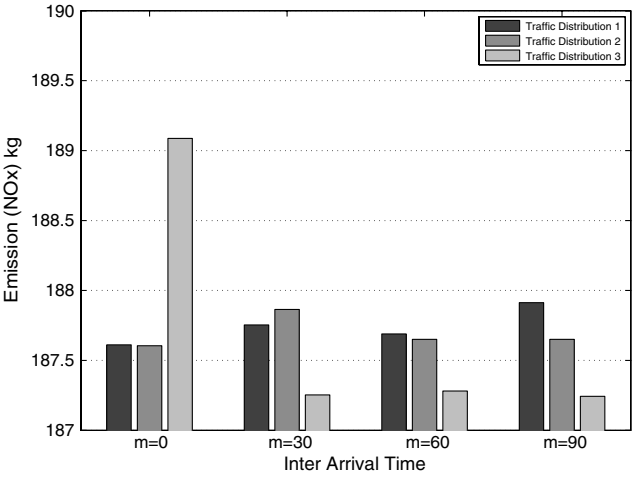

Fig. 18 Cumulative emission (NO_x) from the outer marker to the final approach fix.

3. Cumulative Noise, Emission, and Fuel Burn

Figures 18–20 show, respectively, the cumulative emission (NO_x), fuel burn, and noise for the three traffic distributions with different interarrival timings. For NO_x emissions, Traffic distribution 3 shows highest emission for interarrival time of 0, as it results in highest hold

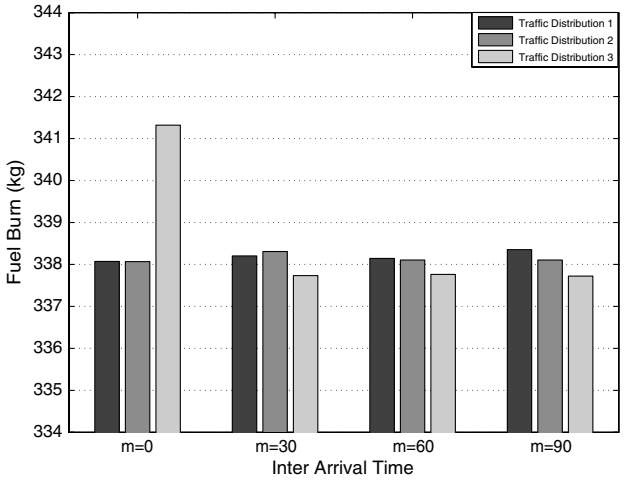

Fig. 19 Cumulative fuel burn from the outer marker to the final approach fix.

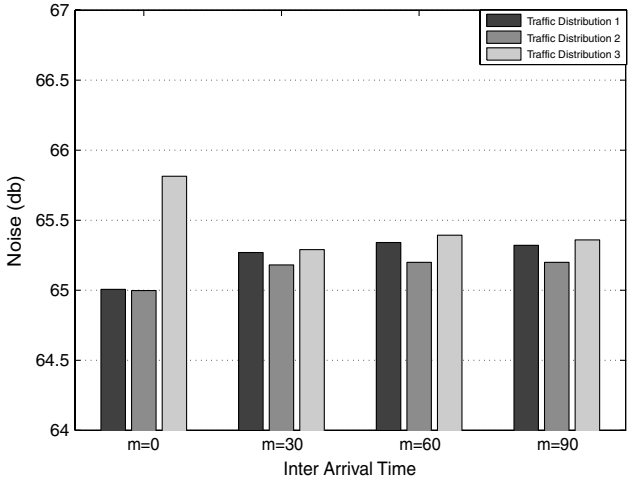

Fig. 20 Cumulative noise from the outer marker to the final approach fix.

patterns, leading to higher fuel burn and emission. However, with increased interarrival timings of 30, 60, and 90, this scenario gives the least emission. A similar pattern is reflected in fuel burn for the three traffic distribution, with traffic distributions 1 and 2 giving similar performance. In terms of noise, scenario 3 remains highest noise contributor, this can be explained by the fact that this scenario requires more spiral routing pattern in the transition airspace to accommodate for the highly concentrated traffic in one area.

VIII. Conclusions

The proposed methodology to generate aircraft-specific dynamic CDA routes that are both laterally and vertically optimized on given objectives (noise, emission, and fuel) from an initial approach fix (IAF) of 10,000 ft to a final approach fix (FAF) of 2000 ft demonstrates that significant savings can be achieved as compared with fixed CDA routes. The use of real-time aircraft position and performance parameters leads to inherently safe CDA routes that can then be converted into a set of artificial waypoints for continuous descent in transition airspace. This approach is designed keeping in mind next-generation jet aircraft, which are appropriately equipped and operate in an ATM environment that supports 4-D trajectory and precession navigation.

The methodology uses the concept of nondominated solutions, where all the routes in this set show the tradeoff between the competing objectives of noise, emission, and fuel burn. By assigning desired weights based on operational priority of each objective and using a simple search algorithm, the desired route can be selected for uplink to the aircraft's flight management systems. These waypoints can then be fed to the flight management systems of the flight and autopilot can execute the CDA maneuver.

The model and the numerical approach used in this paper need further validation by using field-test data. Comparing the flight parameters data from real CDA flights, together with data from noise-monitoring terminals and emission analyzers on the ground, with the simulation data on noise, emission, and fuel burn from the model, can provide more insight into the fidelity of the model.

Another benefit of dynamic CDA with cylindrical representation of transition airspace in rings, levels, and wedges is that it can be easily used for the distribution of aircraft noise in areas surrounding the airport. This can be achieved by blocking a set of wedge points that are to be avoided while generating the set of alternative routes from initial approach fix to final approach fix. This can also be extended to incorporate thunderstorm cells in the vicinity of the airport; however, dynamic blocking of wedge points based on heading, speed, and radar reflectivity of thunder storm cells will be challenging.

The proposed methodology is also extended to accommodate for multiple-aircraft scenario by using time-delay algorithm. 12 different traffic scenarios from three different spatial distribution of traffic and four different interarrival time distribution derived from a Poisson process were investigated on throughout, delay, emission, noise, and fuel. The results gives interesting insight into the interplay of spatial and temporal distribution of traffic and interarrival time and its consequence on throughput and delay of the system.

The dynamic CDA approach has its challenges. It depends largely upon aircraft performance, i.e., meeting speed and altitude restrictions, within the given time of arrival, at artificial waypoints while making a continuous descent. On the operational side, it may lead to reduced controller–pilot communications for level-off segments, but may increase communications for speed constraints. Further coordination between approach and tower controller to achieve dynamic CDA, especially in a traffic constrained environment, will be a challenging task. On the ATC side, there can be a lack of flexibility, since the clearance for the approach has to be given well before the IAF. In the circumstance that a CDA needs to be aborted, it is impossible to resume it, and further radar vectoring will have to be used.

The transition to a dynamic CDA environment will also require use of global navigation satellite systems (GNSS) with distance-measuring equipment (DME) to address loss of navigation at low flight levels in terminal airspace. This and the move toward increased use of GNSS for operational benefits will require mandated carriage of GNSS equipment in all aircraft. The mandate for the carriage of GNSS equipment is in line with the overall strategic context defined by the ICAO communication, navigation, and surveillance (CNS)/ATM concept and the EUROCONTROL GNSS policy. DME and GNSS sensors will be required for all commercial air transport operations in order to meet the operational requirements in respect of the risk of loss of navigation capability on Air Transport CDA operations.

Moreover, implementing CDA in terminal area with a heterogeneous aircraft mix, with current CNS infrastructure, will be challenging. We hope that with the advances in CNS and their integration into Flight Management System, the next-generation aircraft will be a step closer to achieving the Dynamic CDA procedure in terminal airspace. This will certainly require significant investment (in terms of CNS infrastructure and pilot/aircraft certification) and commitment, both from airlines and air navigation service providers.

In terms of infrastructure in advanced air equipment such as cockpit display of traffic information (CDTI), automation-dependent surveillance broadcast (ADS-B) in-and-out capability, DME and GNSS sensors, controller pilot data link control (CPDLC) flight management system integrated with CPDLC will be required. Whereas on the ground, ADS-B ground stations, CPDLC system at approach and control tower, arrival and departure integrated flow-management system, DME and GNSS ground stations, and trajectory prediction with integrated weather are a few examples of the infrastructure and technology required to support this. This will involves significant cost to airlines and air navigation service providers. However, it is expected that in the long run the savings from fuel, increase in airspace capacity and safety with reduced environmental impact will sustain the continued growth in air traffic.

In a study conducted by the United States FAA, the total estimated cost of the ADS-B and CDTI infrastructure and CDA certification (pilots and aircraft) is about $1.8 billion through 2025 in the United States alone. The FAA study also reported that airlines are best to gain from CDA, as it leads to fuel savings of $100,000 per aircraft per annum. In Australia the cost for ADS-B network deployment cost is $14 million and the total rose to $80 million (both in Australian dollars), including necessary telecommunications upgrades.

For future work we will be using demographic data to study the alternative strategies for noise distribution in the community. The impact of emission on local air quality and means to alleviate it will be investigated by incorporating the emission dispersion model. Wind information will be used by storing the wind data in the wedges, and the effect of headwind and crosswinds will be incorporated in dynamic CDA trajectory generation. We will also be looking into Approach and Tower controller coordination issues in implementing dynamic CDAs.

Another challenge lies in implementing CDA operation in a mixed equipage aircraft environment, where aircraft with or without different capabilities (CDPLC, ABS-B, CDTI, etc.) all want to land at the same airport. How to accommodate such heterogenous traffic with a mix of approach procedures (CDA, Step Descent, etc.) will be an interesting research question.

Dynamic CDA trajectory is a step toward realization of 4-D trajectory management in approach and descent phases of flight. Given the inherent uncertainties in air traffic environment and changing objectives of the ATCs, prepublished routes with fixed CDA altitude profiles may not be able to realize the full potential of CDA. Dynamically generated flexible CDA trajectories that are aircraft-specific and are optimized on given objectives (noise, fuel, emissions), that satisfy hard constraints of aircraft performance during descent and approach, and that can meet air traffic constraints (traffic, weather) can provide more efficient use of airspace and increase airport throughput capacity.

Acknowledgments

This work has been cofinanced by the European Organisation for the Safety or Air Navigation (EUROCONTROL) under its University Research Grant program. The content of the work does not necessarily reflect the official position of EUROCONTROL on the matter.

References

[1] Donohue, G., and Laska, W., "United States and European Airport Capacity Assessment Using the GMU Macroscopic Capacity Model (MCM)," *Proceedings of the 3rd USA/Europe ATM R&D Seminar*, Napoli, Italy, June 2000.

[2] "Performance Review Report for 2006," EUROCONTROL, Rept. PRR2006, Brussels, 2007.

[3] Penner, J., *Aviation and the Global Atmosphere*, Intergovernmental Panel on Climate Change (IPCC), Cambridge Univ Press, New York, 1999.

[4] Black, D., Black, J., Issarayangyun, T., and Samuels, S., "Aircraft Noise Exposure and Resident's Stress and Hypertension: A Public Health Perspective for Airport Environmental Management," *Journal of Air Transport Management*, Vol. 13, No. 5, 2007, pp. 264–276. doi:10.1016/j.jairtraman.2007.04.003

[5] Warren, A., Tong, K., Manage, B., and Seattle, W., "Development of Continuous Descent Approach Concepts for Noise Abatement," *Proceedings of the 21st AIAA/IEEE Digital Avionics Systems Conference*, Vol. 1, 2002, pp. 1E3-1–1E3-4.

[6] Melrose, A., "'Basic' Continuous Descent Approach," Airports and Environmental Management Unit, EUROCONTROL, Brussels, 2004.

[7] Wubben, F., and Busink, J., "Environmental Benefits of Continuous Descent Approaches at Schiphol Airport Compared with Conventional Approach Procedures," National Aerospace Laboratory/NLR, Rept. NLR-TP-2000-275, Amsterdam, 2000.

[8] Clarke, J., Ho, N., Ren, L., Brown, J., Elmer, K., Tong, K., and Wat, J., "Continuous Descent Approach: Design and Flight Test for Louisville International Airport," *Journal of Aircraft*, Vol. 41, No. 5, 2004, pp. 1054–1066. doi:10.2514/1.5572

[9] "Concept of Operations for the Next Generation Air Transportation System Ver. 2.0," Joint Planning and Development Office, Washington, D. C., 2007.

[10] Reynolds, H., Reynolds, T., and Hansman, R., "Human Factors Implications of Continuous Descent Approach Procedures for Noise Abatement in Air Traffic Control," *Proceedings of the 6th USA/Europe Air Traffic Management R&D Seminar*, Baltimore, MD, June 2005.

[11] Alam, S., Abbass, H., and Barlow, M., "Air Traffic Operations and Management Simulator ATOMS," *IEEE Transactions on Intelligent Transportation Systems*, Vol. 9, No. 2, 2008, pp. 209–225. doi:10.1109/TITS.2008.922877

[12] Upham, P., Maughan, J., and Raper, D., "*Towards Sustainable Aviation*, Earthscan, London, 2003.

[13] Schumann, U., "Aircraft Emissions," *Encyclopedia of Global Environmental Change*, Wiley, Chichester, England, U.K., 2002, pp. 178–186.

[14] "Continous Descent Approach: Implementation Guidance Information," Environmental Unit, EUROCONTROL, Brussels, 2007.

[15] Anderson, L., and Warren, A., "Development of an Advanced Continuous Descent Concept Based on a 737 Simulator," 21st AIAA Digital Avionics System Conf., AIAA Paper 96-1768, Irvine CA, Oct. 2002.

[16] *Manual of Air Traffic Services Data Link Applications*, International Civil Aviation Organization, Doc. 9694-an/955 ed, Montreal, 2007.

[17] Spence, C. (ed.), *FAA Aeronautical Information Manual/Federal Aviation Regulation*, McGraw–Hill, New York, 2003.

[18] "User Manual for Base of Aircraft Data (BADA)," Rev. 3.6, EUROCONTROL Experiment Centre, Bretigny, France, 2004.

[19] Pietrzko, S., and Hofmann, R. F., "Mathematical Modelling of Aircraft Noise Based on Identified Directivity Patterns," 2nd AIAA/CEAS Aeroacoustics Conf. AIAA Paper 96-1768, June 1996.

[20] Lilley, G., "The Prediction of Airframe Noise and Comparison with Experiment," *Journal of Sound and Vibration*, Vol. 239, No. 4, 2001, pp. 849–859. doi:10.1006/jsvi.2000.3219

[21] Olmstead, J., Fleming, G., Gulding, J., Roof, C., Gerbi, P., and Rapoza, A., "Integrated Noise Model (INM) Version 6.0 Technical Manual," Office of Environment and Energy, Federal Aviation Administration, Rept. FAA-AEE-02-01, 2002.

[22] Dobrzynski, W., Ewert, R., Pott-Pollenske, M., Herr, M., and Delfs, J., "Research at DLR Towards Airframe Noise Prediction and Reduction," *Aerospace Science and Technology*, Vol. 12, No. 1, 2008, pp. 80–90. doi:10.1016/j.ast.2007.10.014

[23] Fink, R., "Airframe Noise Prediction Method," Federal Aviation Administration, Rept. FAA-RD-77-29, 1997.

[24] "ICAO Engine Exhaust Emissions Databank," International Civil Aviation Organization, Doc. 9646-AN/943, Montreal, 1995.

[25] DuBois, D., and Paynter, G., "'Fuel Flow Method 2' for Estimating Aircraft Emissions," Society of Automotive Engineers, Paper 2006-01-19872006.

[26] Sutkus, D. J., and Baughcum, S. L., and DuBois, D. P., "Commercial Aircraft Emission Scenario for 2020: Database Development and Analysis," NASA CR-2003-212331, 2003.

[27] Norman, P. D., Lister, D. H., Lecht, M., Madden, P., Plaisance, C., and Renger, K., "Development of the Technical Basis for a New Emissions Parameter Covering the Whole Aircraft Operation: NEPAIR," European Commission, Rept. G4RD-CT-2000-00182, Brussels, 2003.

[28] Pham, V., Tang, J., Alam, S., Lokan, C., and Abbass, H., "Aviation Emission Inventory Development and Analysis," *Environmental Modelling & Software*, Vol. 25, No. 12, 2010, pp. 1738–1753. doi:10.1016/j.envsoft.2010.04.004

[29] Zitzler, E., Thiele, L., Laumanns, M., Fonseca, C. M., and da Fonseca, V. G., "Performance Assessment of Multiobjective Optimizers: An Analysis and Review," *IEEE Transactions on Evolutionary Computation*, Vol. 7, No. 2, 2003, pp. 174–188. doi:10.1109/TEVC.2003.810761

[30] Abbass, H., "The Self-Adaptive Pareto Differential Evolution Algorithm," *Congress on Evolutionary Computation (CEC '02)*, Vol. 1, 2002, pp. 831–836.

[31] Mohleji, S., "Curved Approaches in the Netherlands: Feasibility and Benefits," Massachusetts Inst. of Technology Research Establishment, Rept. MTR99W99W122, Bedford, MA, 1999.

[32] Wennerberg, A., and Gibellini, M., "Time-Based Separation: CDG Real-Time Simulation Results," EUROCONTROL Experimental Centre, Rept. 17/06, Bretigny, France, 2006.

[33] *Designated Airspace Handbook*, Air Services Australia, Canberra, Australia, Nov. 2004.